12th International Workshop on Wave Hindcasting and Forecasting, Kohala Coast, Hawai'i, HI, 2011.

CALIBRATION OF THE "IOWAGA" GLOBAL WAVE HINDCAST (1991–2011) USING ECMWF AND CFSR WINDS

Fabrice Ardhuin[1], Jenny Hanafin,
Yves Quilfen, Bertrand Chapron, Pierre Queffeulou, Mathias Obrebski
IFREMER, Laboratoire d'Oceanographie Spatiale, Plouzané, FRANCE

Joseph Sienkiewicz
NOAA/NCEP, Ocean Prediction Center, Camp Springs, MD
Doug Vandemark
University of New Hampsire, Durham, NH

1 Introduction

Numerical wave models have traditionnally been calibrated mostly in terms of wave heights, and to a lesser extent peak periods and directions. However, new applications require the validation of air-sea fluxes [e.g. Il-Ju Moon et al., 2004], higher order spectral moments such as the surface Stokes drift and mean square slopes [e.g. Tran et al., 2010], and spectral shape parameters that control the second order spectrum which is responsible for driving long waves and generating seismic noise [e.g. Reniers et al., 2010, Ardhuin et al., 2011a]. Physical parameterizations have been proposed recently that capture some of the variability of the high frequency spectral levels, and these also lead to more accurate results for the dominant waves [Ardhuin et al., 2010]. Based on this experience, we expect that improvements for specific applications will generally lead to benefits for all users of numerical wave models. Also, the validation of many different parameters estimated from wave spectra may also provide some constraints on the otherwise 'free parameters' that are still too many in wave generation and dissipation parameterizations. With these ideas in mind, we are pursuing the development of new parameterizations as part of the National Ocean Partnership Program operational wave model improvement project [Tolman et al., 2011]. In particular, wave breaking statistics are used to improve on the parameterization of wave dissipation [Leckler et al., 2011].

Leaving out wave breaking properties, we focus on other parameters and present here some preliminary result from the project "Integrated Ocean Waves for Geophysical and other Applications" (http://wwz.ifremer.fr/iowaga). The numerical model used for this is a global implementation of WAVEWATCH III(R) version 4.04, using the parameterization 'TEST441b' described in detail in Ardhuin et al. [2010]. This parameterization has now been used for the last three years as part of the Previmer forecasting system (http://www.previmer.org/), using operational wind analyses and forecasts from ECMWF, with multi-grid systems and stand-alone unstructured grids [e.g. Ardhuin et al., 2009]. Results from the regular grids appear under the 'SHOM' tag in the JCOMM model inter-comparisons [e.g. Bidlot, 2009]. Monthly validation reports have shown excellent performance against buoy data, typically producing the smallest errors for forecast ranges of 48 hours and beyond. This has lead Meteo-France to adapt the same physical parameterization in their new operational wave forecasting system in 2010, and test are under way at NOAA/NCEP for a possible use in operations. One of the issues faced by NCEP is the longer CPU time for the new parameterizations, which make the full model about 40% more expensive than using the parameterization by Tolman and Chalikov [1996]. This cost is due to non-isotropic dependence of dissipation rates for one component on the energy of other components and their associated breaking probabilities, which requires the calculation of convolution integrals over part of the two-dimensional spectrum.

[1] E-mail:ardhuin-at-ifremer.fr

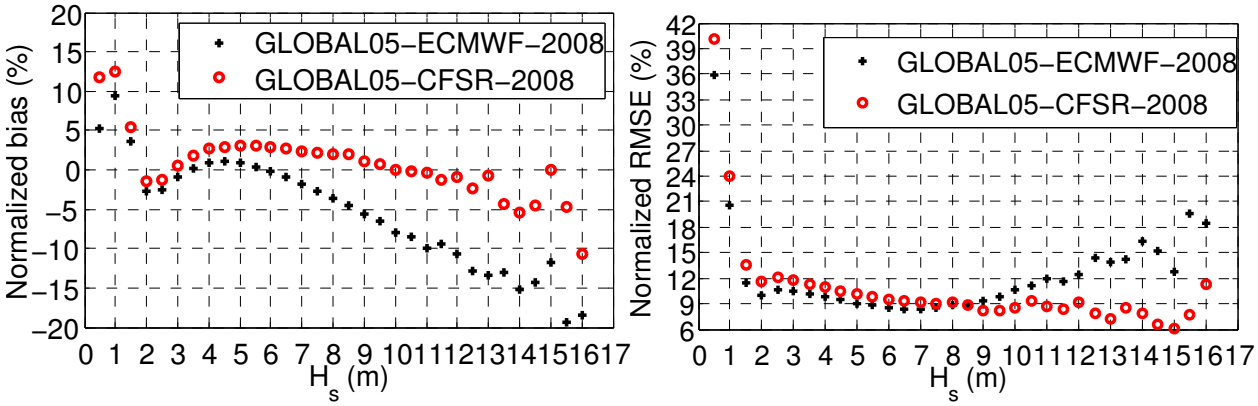

Fig. 1 : Normalized bias for H_s against altimeter data, as a function of H_s, for the years 1991 to 2001.

Our purpose here is to provide some guidelines for adjusting the model parameters when using other sources of wind forcing, and give further validation of the model in terms of other parameters. We particularly investigate the impact of using different wind fields, the ECWMF operational analyses and the recent Climate Forecast System Reanalysis [Saha et al., 2010]. A preliminary hindcasts for the years 2002-2009 has been carefully validated using altimeter data and used to validate the importance of icebergs for waves in the Southern Ocean [Ardhuin et al., 2011b]. We have now extended the period to the beginning of the continuous satellite altimeter record, with ERS data, in 1991. This altimeter data provides an important check on the possible spatial and time-varying bias introduced by the wind forcing. In our hindcast, only the years 2002–2009 include a damping caused by icebergs in the Southern Ocean. This will be corrected as soon as the CERSAT iceberg database is extended in time. The full hindcast database is accessible in NetCDF format via ftp (`http://tinyurl.com/yetsofy`). Further extensions, for years before 1991, are being tested, using seismic noise data to detect and correct time-varying biases at basin scale, in addition to local buoy validation.

2 The hindcast: models and forcings

2.a Description of models

The model results described here are obtained with a 0.5° resolution grid in latitude and longitude, and a spectral resolution with 24 directions and 32 frequencies from 0.037 to 0.72 Hz. A diagnostic f^{-5} tail is imposed only above 9.9 times the mean frequency, which generally falls outside the model frequency range, so that the estimates of mean square slopes are practically not affected by this tail. The main features of the TEST441b parameterizations are:

- Following Tolman and Chalikov [1996], a well separated dissipation of swell (negative wind input) and dissipation due to breaking
- A non-linear swell dissipation based on SAR-derived dissipation rates across the Pacific [Ardhuin et al., 2009]
- Following Phillips [1984], a breaking-induced dissipation that is based on the local saturation spectrum, but anisotropic with a higher dissipation rate in the mean wave direction. That latter aspect was designed to fit observed directional spreadings.
- A cumulative dissipation rate inspired by Babanin and Young [2005] but directly estimated from breaking wave probabilities. This dramatically enhances the dissipation at frequencies above 3 times the peak frequency.
- a reduced wind input at high frequencies compared to Janssen [1991], and an intermediate input level at the peak, compared to the higher values with Janssen [1991] and much lower values with Tolman and Chalikov [1996].
- the Discrete Interaction Approximation [Hasselmann et al., 1985] for the non-linear interactions.

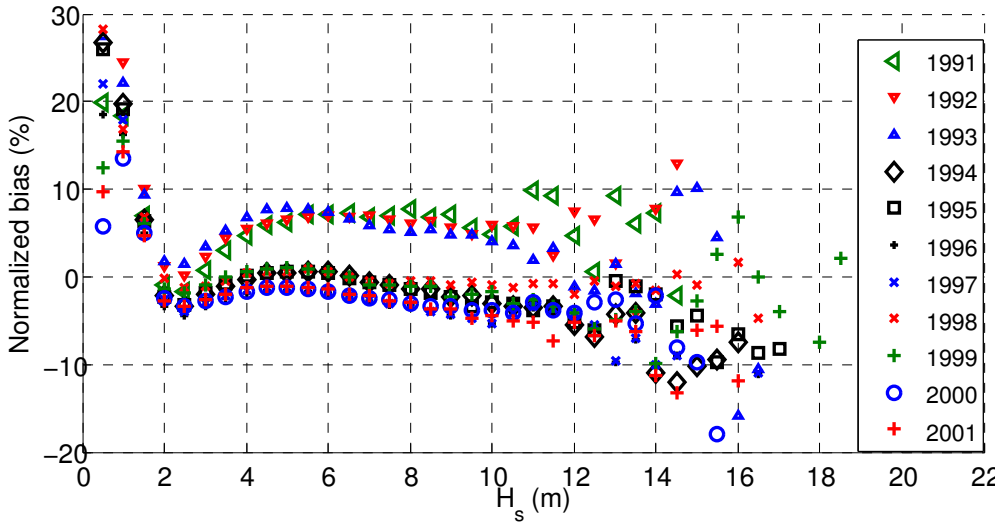

Fig. 2 : Normalized bias and normalized RMSE for H_s in 2008 against altimeter data, as a function of H_s.

The modelled grids include

- A global multi-grid system with a baseline 0.5° resolution in latitude and longitude, with zooms on the North-West European shelf at 0.1°, West Indies (Puerto Rico to Venezuela), Tuamotus, New Caledonia, U.S. East Coast and Gulf of Mexico at 0.2°, French Atlantic coast at 1/30°. At the time of writing, the full time period has only been run on a single grid 0.5°, and only the period 2002-2011 has been run with the multi-grid system.
- A Mediterranean multigrid system, with a baseline 0.1° resolution split in a Mediterranean and a Black Sea grids, and a 1/30° French Mediterranean domain, including Corsica.
- An unstructured grid (resolution 100 m to 5 km) over the Iroise sea, including currents and water levels, for the years 2002-2011.

Other unstructured grids used for the routine Previmer forecasts will probably also be used for hindcasts.

The built-in shortcomings of this parameterization is that the dissipation rate near the peak is local in frequency. Given the higher saturation level at the peak, this leads to a strong peak in the dissipation rate that is not consistent with breaking statistics [Leckler et al., 2011]. Also, the relative weak input level tends to produce mean directions in slanting fetch conditions that are too oblique relative to the shoreline.

We note that the model was ran with 10-m winds, without any air-sea stability correction. Absolutely no wave measurement, direct or indirect, was assimilated in the model. In contrast, many observations from satellite altimeter and SAR to buoys and seismic noise spectra were used to calibrate the model parameters over the year 2008 [Ardhuin et al., 2010, 2011a].

2.b Differences with ECMWF or CFSR winds

As a result of our forcing choices, the hindcasts contains some discontinuities due to the effects of icebergs. That latter effect was minimized by adjusting the wind-wave growth parameter $\beta_{\max} = 1.52$ used for ECMWF winds, to $\beta_{\max} = 1.33$ for CFSR or NCEP analyses. To avoid confusion the parameterization with $\beta_{\max} = 1.33$ is called TEST441f. This adjustment compensates the high relative bias of CFSR winds for average values. This adjustment was calibrated for the year 2008 and was found to give good results for the years 1994 to 2009.

However, due to a different shape in the histogram of high winds, this calibration cannot correct biases equally for the full range of wave heights. Interestingly, the strength of high winds in CFSR, compared to ECMWF analysis, reduces the negative bias for very high ($H_s > 9$ m) and phenomenal seas ($H_s > 14$ m), and allows a remarkable reduc-

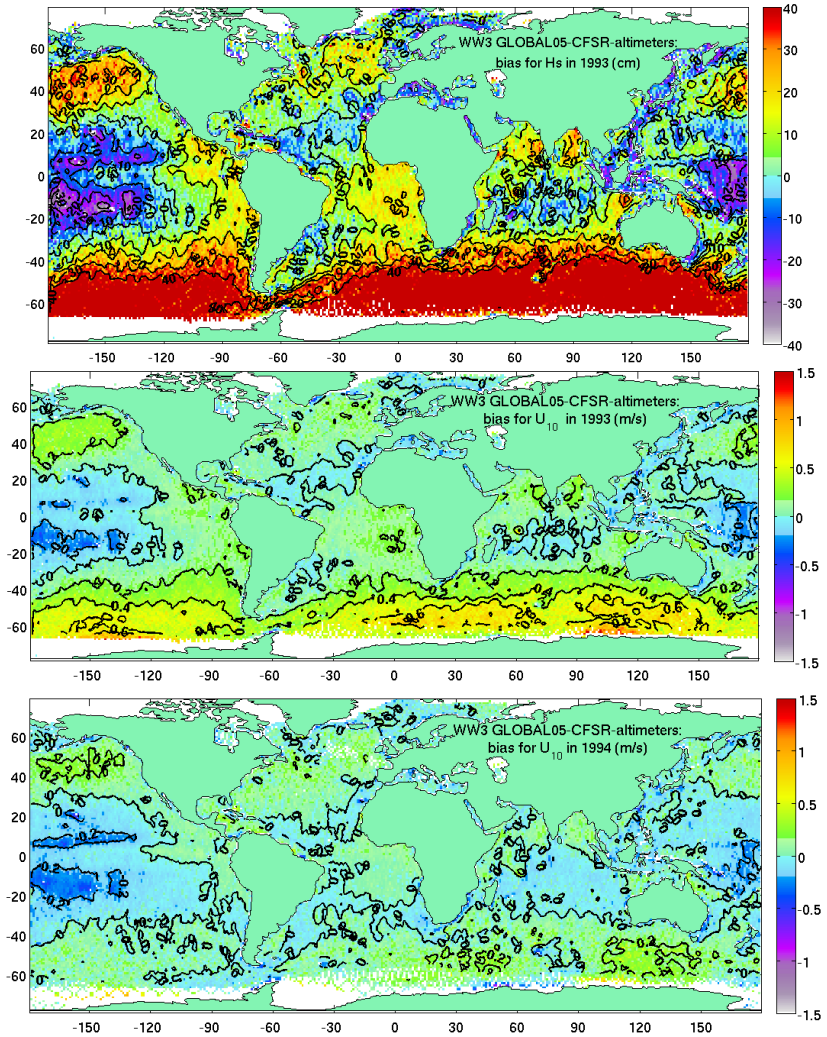

Fig. 3 : Top panel: Bias in cm for H_s in 1993, against altimeter data from ERS-1 and Topex/Poseidon. Middle panel, bias of CFSR winds in 1993 against the same altimeter sources. Bottom, same wind speed bias for year 1994.

tion in root mean square (rms) errors for the highest waves, even though the random errors are larger in 2008 when using CFSR winds (figure 1).

We have thus decided to use CFSR winds as a baseline, and also use ECMWF wind analyses for the years 2006-2011, in order to benefit from lower random errors, and the immediate availability of the wind fields. We have thus included complementary model results for 2006–2009 with ECMWF winds. Uncorrected results with CFSR winds may be preferred for the estimation of extreme events, but a correction of results with ECMWF winds may still produce smaller random errors for 2006–2011.

2.c Time-varying biases from 1991 to 2011

The spatial pattern of biases is fairly constant for the years 2002 to 2009 for which we have used a masking by small icebergs[Ardhuin et al., 2011b]. For the years 1991 to 2001, figure 2 shows that there is a 2% bias shift for the years 1994, 1995, 1998, 1999 compared to 1996, 1997, 2000 and 2001. But more importantly, it reveals a very strong anomalous bias (about 10%) for the years 1991 to 1993.

This bias can be seen both in altimeter data, at the global scale, and in buoy data from the U.S. coast, in particular at the 46211 buoy, operated by CDIP.

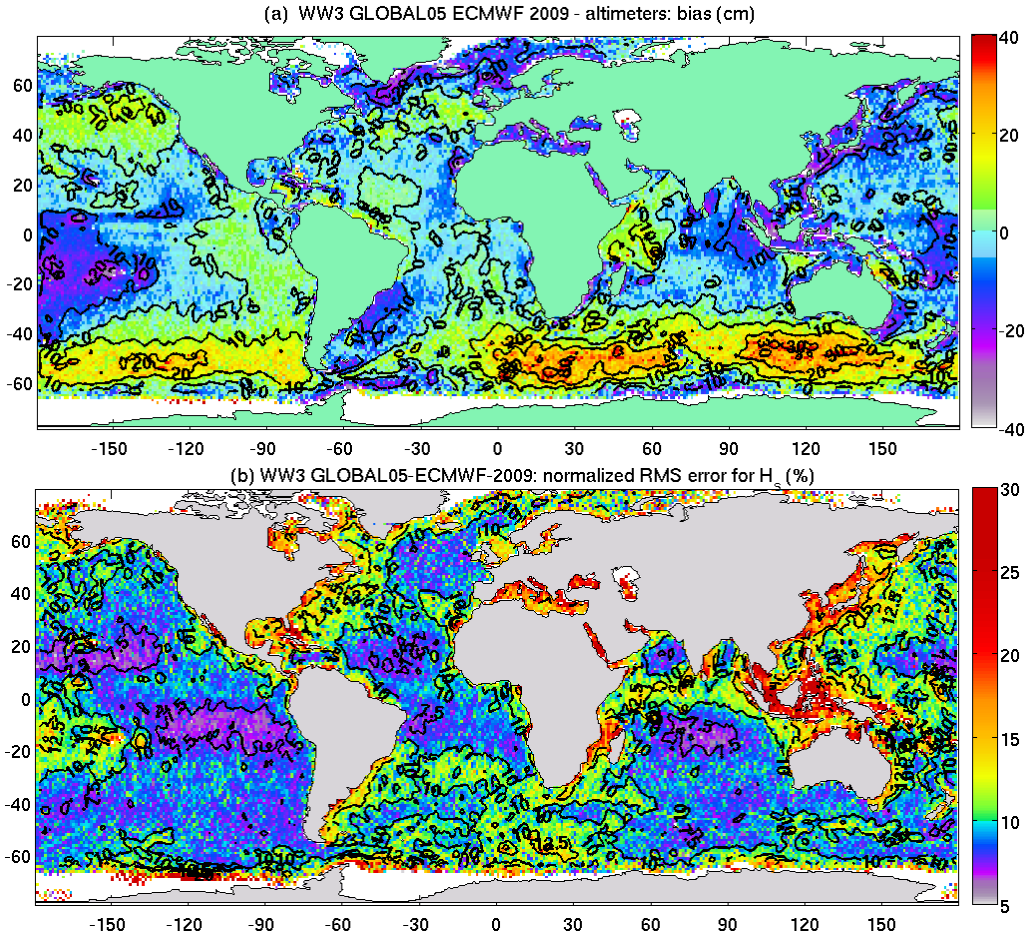

Fig. 4 : (a) Bias and normalized (b) RMS error for the modeled significant wave heights for the year 2009, against data from Jason-1, Jason-2 and Envisat altimeters. Both model and altimeter data are averaged along the satellite tracks over 1 degree in latitude. There are 2.4 million averaged values.

At that buoy the model bias exceeds 17% for H_s for these years, compared about 3% for the years 2004–2008 (not shown).

The examination of CFSR winds and waves compared to altimeter data shows that the errors are strongest over the Southern ocean (top panel in figure 3) and disappear in 1994. This pattern is clearly associated with a change in wind speed biases for the years 1991–1993, up to 1 m/s right around Antarctica (middle panel in figure 3), and a weaker bias in the North Pacific, compared to more realistic values in 1994 (bottom panel in figure 3) and the following years (not shown).

Looking at the details of the data used in the CFSR analysis, we can see that 1994 corresponds to the start of SSM-I wind speed assimilation [figure S14 in Saha et al., 2010]. It thus appears that SSM-I data has a beneficial impact, reducing the high bias of high winds in the sub-polar regions. So far we have left the 1991-1993 results uncorrected. It is possible that a correction of the CFSR wind speed histogram may be enough to correct the biases on wave parameters.

For the years before 1991, in the absence of global validation data from satellite altimeters, it is difficult to guarantee the stability of biases for the modeled wave parameters.

Ongoing work on the use of seismic noise data [e.g. Ardhuin et al., 2011a] should provide a reliable bias estimator at global scales, which is readily available back to the early 1980s, when numerical seismic data is available. Going further back in time will require

a careful and well planned effort for digitizing old seismograph data [e.g. Grevemeyer et al., 2000], with some data sources going back to the late 19th century [Algué, 1900].

3 Validation

3.a Significant wave heights

For the full altimeter era, patterns in model error are similar to what is shown on figure 4. Using CFSR winds for the years 1994–2009, the positive bias for H_s in the Southern Ocean is increased by 5 to 10 cm. This local pattern is consistent with relatively strong high winds in CFSR. Overall, random errors are smallest in the recent years and with ECMWF wind fields. This is the reason why we chose to show results for 2009 on figure 4, for which the errors are least. With CFSR winds, there is also a slow decrease of random errors with time from 1994 to 2001. At this stage we have not sought to discriminate the source of that trend, between more accurate wind fields and more accurate altimeter measurements.

Besides obvious low biases in the Northern Mediterranean, Black Seas and Indonesian archipelago, which may be largely attributed to wind errors and a coarse model resolution, we note persistent low biases to the South-East of Greenland, east of Argentina, east of India to the south-east of Australia and New-Zealand, and in the South-West Pacific.

There are probably several factors that contribute to this low bias, one of them being the relatively slow growth of the of young waves, in the model, in particular for short fetches [Ardhuin et al., 2010]. Some early validation tests of the spatial distribution of swell fields also showed that the model had a tendency to produce swells in a range of directions that is more narrow than what is observed from space [Delpey et al., 2010].

Because the dominant weather systems have winds to the East, a too narrow swell distribution will fail to send energy towards the east coasts. This may be related to diffraction or some unresolved scattering effects, as suggested by the apparent turning of swells behind large island groups such as French Polynesia (Fabrice Collard, personal communication 2008).

Another outstanding problem is the change from a low H_s bias for $H_s > 2$ m to a high bias for $H_s < 2$ m (figure 1). These biases yield a histogram of H_s that is very peaked at 2 m, and unrealistic. This problem may be due to the transition in from a laminar to a turbulent boundary layer. In our swell dissipation parameterization, this transition includes a discontinuity in the air-sea friction factor.

3.b Mean square slopes (mss)

Either from model or satellite altimeter, the estimates of the mss are indirect but they provide an interesting check on the variability spectral tails, which is very much controlled by the cumulative dissipation term [e.g. Leckler et al., 2011].

Here we estimate a mss from Ku band cross section as

$$\mathrm{mss_{Ku}} = \frac{0.48}{\exp\left[(\sigma_0 + 1.4) \times (0.1 \log(10))\right]} \qquad (1)$$

where σ_0 is the normalized radar cross section as provided in the Globwave homogenized dataset [Queffeulou and Croizé-Fillon, 2010], 1.4 is a bias correction in dB, and 0.48 is an effective Fresnel coefficient [Chapron et al., 2000].

For the model, a corresponding mss is extrapolated from the mss ($\mathrm{mss_{3m}}$) integrated over the limited frequency range of the model which as a maximum frequency of 0.72 Hz that corresponds to a wavelength of 3 m. For this we use an expression adapted from Vandemark et al. [2004],

$$\mathrm{mss_{Ku,model}} = \mathrm{mss_{3m}} + 0.0035 + 0.0093 \log(U_{10}) \qquad (2)$$

with

$$\mathrm{mss_{3m}} = \int_0^{2\pi} \int_0^{0.72\ \mathrm{Hz}} k^2 E(f,\theta) \mathrm{d}f \mathrm{d}\theta \qquad (3)$$

Figure 5 shows that the variability of the mss as a function of wind speed and wave height using satellite data, and also taking one example offshore of California, with NDBC buoy 46013. In order to test the impact of the buoy sensor quality, we also used winds from buoy 46013 with wave data from a nearby Datawell Waverider buoy (WMO code 46214, operated by the Coastal Data Information Program). When offshore waves are removed, we get a similar pattern of mss variation with wind speed and H_s. When the Jason-1 wind is used, one recovers the geophysical model function (GMF) used to estimate the wind speed from σ_0 and H_s. Unfortunately the GMF chosen for Jason does not include the full variability os σ_0 with sea state for low wind speeds [e.g. Gourrion et al., 2002]. Comparison with Quikscat winds (Fabrice Collard, personal communication 2011) shows that the true distribution of $\mathrm{mss_{Ku}}$ with wind and wave height is closer to what is shown in the central panel of figure 5, when

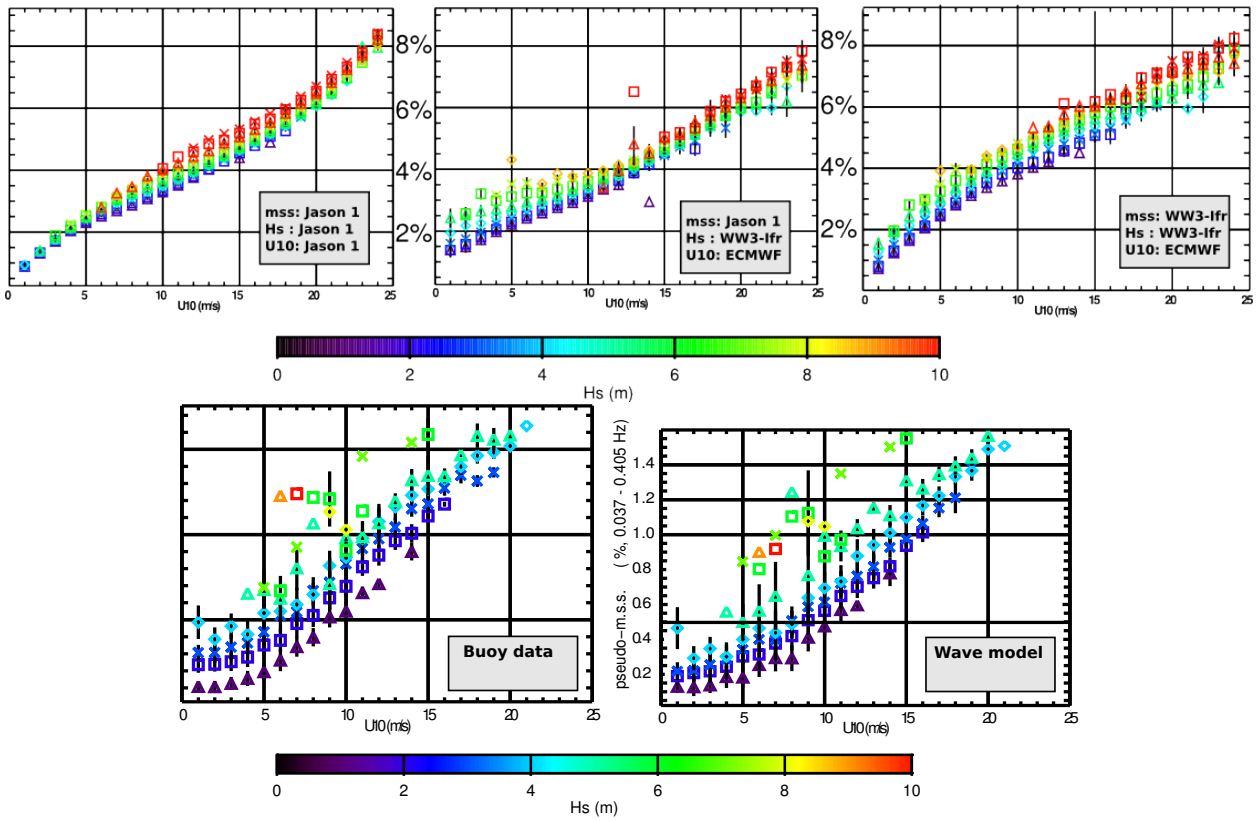

Fig. 5 : Comparison of mss distributions (on the vertical) as a function of wind speed (U_{10}) and significant wave height (H_s) for the year 2008. Top line, for the global ocean, on the left is the distribution using only Jason data, but this means that the wind speed is not an independent estimate as it is derived from σ_0 and H_s using a geophysical model function. In the central plot, U_{10} is given by ECMWF analyses and on the right, mss and H_s are given by the wave model. Bottom line, for the buoy 46013, off Central California using (a) the buoy data and (b) the wave model, using a high frequency cut-off at 0.4 Hz.

---

the Jason-derived wind is replaced by ECMWF wind analyses.

Comparing the top and bottom panels shows that a little more than 10% of the Ku-band mss is accounted for by waves of frequencies less than 0.4 Hz, i.e. wavelengths more than 10 m, and the mss variability from satellite data is comparable to the mss estimated from the buoy spectrum up to 0.4 Hz, showing that fairly long waves ($L > 10$ m) account for a large part of the variability of the $\mathrm{mss_{ku}}$ that is not due to winds.

The top-right and bottom-right panels show that the model is able to predict most of the variability that is observed. For wind speeds above 10 m/s the mss is overestimated by the wave model using the transformation given by eq. (2). The analysis of buoy data suggests that this overestimation is a real model effect, and not an artifact of the interpretation of the altimeter σ_0. The modeled mss_{3m} at low winds has a relatively low bias by 0.05 percentage points at the location of buoy 46013.

A similar low bias off the California coast is also found when comparing the model to altimeter data (figure 6). It is difficult to validate the global distribution of mean square slopes with buoys, given their very sparse distribution, and this is where the altimeter data is very useful. Once the regional biases are removed, the relative error in the estimate of $\mathrm{mss_{Ku}}$ varies around 13% (figure 6), which is almost as low as the error on H_s, around 10%.

4 Hindcasts of extra-tropical storm Quirin: what trust in wave models up to $H_s = 20$ m?

Given the very different behavior of wave height bi-

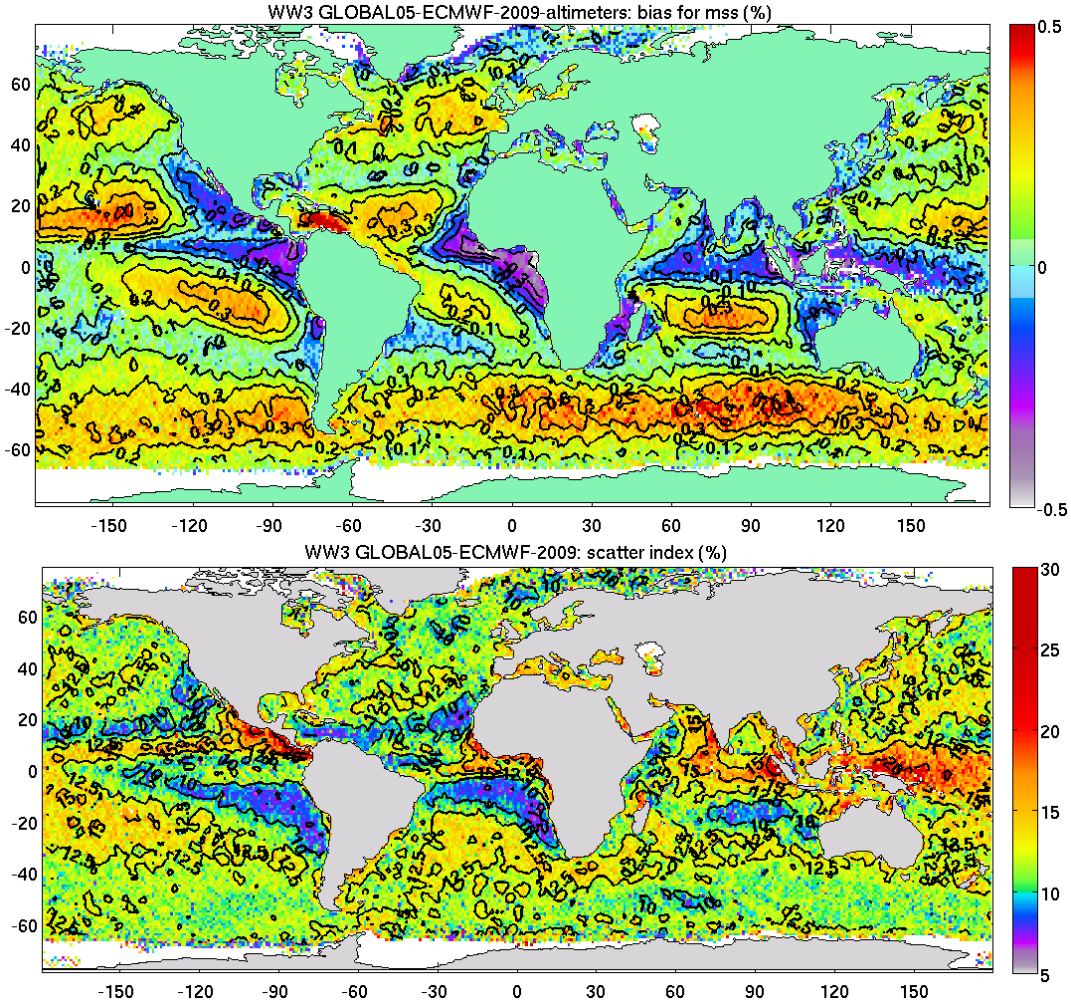

Fig. 6 : Top: Bias of the model estimations of mss given by eq. (2), after a reduction by 10%, against altimeter data using eq. (1). Bottom: Scatter index for the model estimation of mss (this is the normalized RMS error after bias correction).

ases for very high and phenomenal seas when shifting from CFSR to ECMWF winds (figure 1), we have made a preliminary investigation of the source of this bias: is the wind too low, or, as suggested by Cavaleri [2009], is there any systematic problem in the wave model that would make it 'miss the peaks'? For this we jumped on the occasion given by a recent event, with the largest sea state ever recorded by a satellite altimeter.

Although wave models have seldom been validated for extreme wave heights, some numerical hindcasts studies have shown a good consistency of very high wave heights, up to $H_s = 20$ m with satellite measurements, provided that the winds used to drive the wave model are made consistent with observations [Cardone et al., 2009]. The 2011 storm Quirin generated wave with a record-breaking maximum value of $H_s = 20.12$ m reported by Jason 2 on February 14 at 11:03:09 UTC, at location 29.57W 49.17 N (cycle number 96, pass number 139, 1 Hz data). This number is the uncorrected value in the NASA/CNES product. This exceeds the maximum in the 2007 event discussed in Cardone et al. [2009], which has been reprocessed by NASA and CNES to 'only' $H_s = 19.13$ m. The wind and waves of Quirin are investigated in detail in Hanafin et al. [2011], which is summarized below.

This particular storm moved rapidly across the north Atlantic, with a minimum sea level pressure deepening from 984 hPA on 13 February at 0000

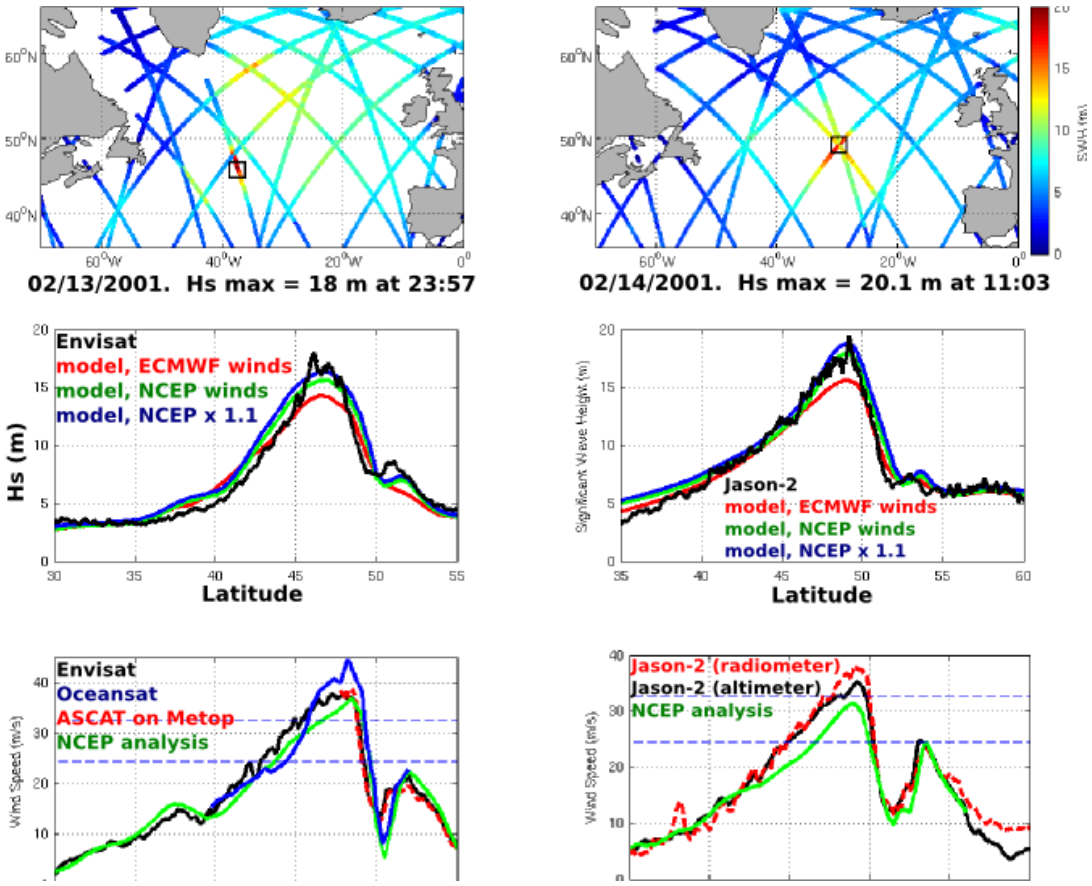

Fig. 7 : Top: altimeter significant wave heights along the tracks of Geosat, Jason-1/2 and Envisat, on February 13th 2011 (left panel) and February 14th 2011 (right panel). The black squares indicates the location of the most extreme sea states measured during for each of these days by the Envisat and Jason-2 altimeter, respectively. Middle: H_s along the Envisat (left) and Jason-2 (right) altimeter tracks. Bottom: Wind speed interpolated on the Envisat (left) and Jason-2 (right) altimeter tracks. All estimates have been computed at the NCEP spatial resolution. The two dashed blue lines give the limits of tropical storm force winds ($U_{10} = 24.5$ m/s) and hurricane-force winds ($U_{10} = 32.7$ m/s).

UTC, to 950 hPA, 24 hours later. The Quikscat-type scatterometer onboard Oceansat recorded hurricane-force winds ($U_{10} > 32.7$m/s) over a region of about 700 km in diameter, and a maximum wind speed of 45 m/s. This extreme value cannot be verified but we obtain coherent information from other remote sensors (Jason-2 and Envisat altimeters, ASCAT scatterometer) for the extent of the hurricane-force winds (figure 7). These other measurements are certainly more accurate for these high wind speeds [Quilfen et al., 2011].

Around the peak of the storm, the operational analyses from NCEP haves wind speeds that are typically 10% lower than the remotely sensed estimates (figure 7), and ECMWF values are even lower. Similarly to the case studied by Cardone et al. [2009], these underestimated winds are the likely reason for the low wave height bias E in this particular case.

Although several more storms should be studied, this pattern of underestimation of the most severe winds, more pronounced for ECMWF than for CFSR or NCEP analysis, is the likely reason for the low bias of H_s for the largest values, as shown in figure 1.

This conclusion was further tested by increasing the

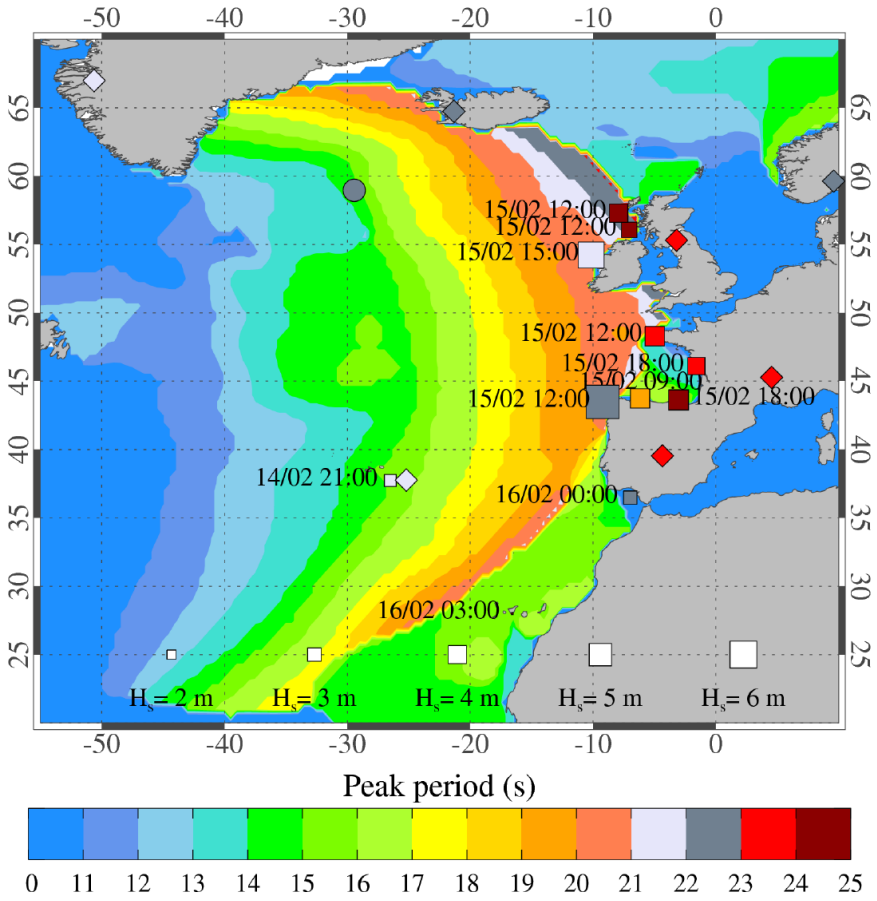

Fig. 8 : Peak periods as calculated by the model with enhanced NCEP wind analyses (background colors), and measured by Envisat's ASAR in wave mode (circles), wave buoys (squares) and seismic stations (diamonds: SFJD - Greenland, CMLA - Azores, ESK - Scotland, SSB - France, PABO - Spain, and KONO - Norway). The model output is shown for 12:00 UTC on February 15th, as the longest swells were encroaching on the west coast of Scotland. Buoy and seismic data correspond to the time of maximum T_p, with the time indicated on the plot, and the SAR data was acquired on February 14th and reprocessed from level 1 data since this very long swell is removed by the operational level 2 processing.

NCEP wind speeds by 10% over the full model domain, and re-running the model for the month of February 2011. The results with these enhanced winds are now in very good agreement with the measured heights, and are rather slightly higher in terms of wave height. Also, the very large peak periods observed at European buoys and recorded by seismic stations, from 21 to 25 s, are also well reproduced by the model (figure 8 and table 1). All these measurements have been inspected for quality. Among these

Surfer Benjamin Sanchis was more lucky and took the 2011 worldwide biggest wave prize for his run down one of these waves on February 16 on

the Datawell Waverider with WMO code 62069, owned by Ifremer, operated by CETMEF, and situated at 4.97 W and 48.29 N recorded a peak period of 23.5 s and 4.4 m.

These very long periods made this sea state truly special. One of our colleagues, Abel Balanche, escaped with a few bruises after underestimating the power of the swell while surfing near Brest.

the Belhara reef, off the south-west French coast (http://www.billabongxxl.com/biggest_wave_nom/index_5.html). There were also some occa-

sional damage associated with a 1 m seiche set up by strong infragravity waves in the usually quiet harbor or Royan, France.

5 Conclusions

A 20 year hindcast of global wave parameters has been produced using new parameterizations for wave dissipation [Ardhuin et al., 2010], and forcing from a combination of ECMWF analysis and CFSR reanalyses, sea ice from CFSR and ECMWF and icebergs from CERSAT. The continuous validation with altimeter and buoy data reveals several important facts,

- CSFR and NCEP analyses have systematically higher values than ECMWF analyses of the wind speed, and this is even more true for the highest speed range.
- a simple calibration of the wind wave growth parameter, $\beta_{\max} = 1.33$ for CFSR or NCEP winds compared to $\beta_{\max} = 1.52$ for ECMWF winds corrected the average to high wave heights.
- Modeled wave heights are still too low for the highest values ($H_s > 12$ m), likely due to an underestimation of the winds in these conditions.
- the mean square slope of the sea surface is relatively well estimated with the model, and may be a useful parameter for remote sensing applications.
- CFSR winds are anomalously high in the Southern Ocean for the years 1991–1993, compared to following years, resulting in anomalous high biases for these year, including off the U.S. West coast. This bias is corrected for the following years, probably due to the start of SSM-I data assimilation in CFSR.
- a hindcast of 2011 storm Quirin, which holds the record for the highest ever measured sea state by a satellite altimeter, was well reproduced after correcting for the wind bias. The exceptional swell periods reaching the Atlantic coasts of Europe were also well reproduced.

6 Acknowledgements

We thank all the providers of wind and wave measurements at NDBC, CDIP, SHOM, CNES, NASA, ESA, and ISA that have been critical for assessing the quality of wind and wave models. We thank J.-F. Piolle and M. Accensi for their homogenization of the buoy data formats and work on NetCDF post-processing, and the entire WAVEWATCH III$^{(R)}$ development team, in particular H. L. Tolman, J. H. G. M. Alves, and A. Chawla. This work is supported by a FP7-ERC young investigator grant number 240009 for the IOWAGA project, the U.S. National Ocean Partnership Program, under grant U.S. Office of Naval Research grant N00014-10-1-0383. Additional support from ESA and CNES for the Globwave project is gratefully acknowledged.

References

J. Algué. Relation entre quelques mouvements microséismiques et l'existence, la position et la distance des cyclones à Manille (Philippines). In *Congrès international de Météorlogie, Paris*, pages 131–136, 1900.

F. Ardhuin, L. Marié, N. Rascle, P. Forget, and A. Roland. Observation and estimation of Lagrangian, Stokes and Eulerian currents induced by wind and waves at the sea surface. *J. Phys. Oceanogr.*, 39(11): 2820–2838, 2009. URL http://journals.ametsoc.org/doi/pdf/10.1175/2009JPO4169.1.

F. Ardhuin, E. Rogers, A. Babanin, J.-F. Filipot, R. Magne, A. Roland, A. van der Westhuysen, P. Queffeulou, J.-M. Lefevre, L. Aouf, and F. Collard. Semi-empirical dissipation source functions for wind-wave models: part I, definition, calibration and validation. *J. Phys. Oceanogr.*, 40(9):1917–1941, 2010.

F. Ardhuin, E. Stutzmann, M. Schimmel, and A. Mangeney. Ocean wave sources of seismic noise. *J. Geophys. Res.*, 116:C09004, 2011a. doi: 10.1029/2011JC006952. URL http://wwz.ifremer.fr/iowaga/content/download/48407/690392/file/Ardhuin_etal_JGR2011.pdf.

F. Ardhuin, J. Tournadre, P. Queffelou, and F. Girard-Ardhuin. Observation and parameterization of small icebergs: drifting breakwaters in the southern ocean. *Ocean Modelling*, 39:405–410, 2011b. doi: 10.1016/j.ocemod.2011.03.004.

A. V. Babanin and I. R. Young. Two-phase behaviour of the spectral dissipation of wind waves. In *Proceedings of the 5th International Symposium Ocean Wave Measurement and Analysis, Madrid, june 2005*. ASCE, 2005. paper number 51.

J.-R. Bidlot. Intercomparison of operational wave forecasting systems against buoys: data from ECMWF, MetOffice, FNMOC, NCEP, DWD, BoM, SHOM and JMA, September 2008 to November 2009. Technical report, Joint WMO-IOC Technical Commission for Oceanography and Marine Meteorology, 2009. URL http://www.jcomm-services.org/modules/documents/documents/model_comparison_second_list_200809_200811.pdf. available from http://tinyurl.com/3vpr7jd.

V. J. Cardone, A. T. Cox, M. A. Morrone, and V. R. Swail. Satellite altimeter detection of global very extreme sea states. In *Proceedings, 11th Int. Workshop of Wave Hindcasting and Forecasting, Halifax, Canada*, 2009.

L. Cavaleri. Wave modeling: Missing the peaks. *J. Phys. Oceanogr.*, 39:2557–2778, 2009. URL http://journals.ametsoc.org/doi/pdf/10.1175/2009JPO4067.1.

B. Chapron, V. Kerbaol, D. Vandemark, and T. Elfouhaily. Importance of peakedness in sea surface slope measurements. *J. Geophys. Res.*, 105(C7):17195–17202, 2000.

M. Delpey, F. Ardhuin, F. Collard, and B. Chapron. Space-time structure of long swell systems. *J. Geophys. Res.*, 115:C12037, 2010. doi: 10.1029/2009JC005885.

J. Gourrion, D. Vandemark, S. Bailey, and B. Chapron. Investigation of C-band altimeter cross section dependence on wind speed and sea state. *Can. J. Remote Sensing*, 28(3):484–489, 2002.

I. Grevemeyer, R. Herber, and H.-H. Essen. Microseismological evidence for a changing wave climate in the northeast Atlantic Ocean. *Nature*, 408:349–1129, 2000.

J. Hanafin, Y. Quilfen, D. Vandemark, B. Chapron, H. Feng, and J. SienkiewiCZ. Phenomenal sea states and swell radiation: a comprehensive analysis of the 12-16 February 2011 North Atlantic storms. *Bull. Amer. Meterol. Soc.*, 2011. submitted.

S. Hasselmann, K. Hasselmann, J. Allender, and T. Barnett. Computation and parameterizations of the nonlinear energy transfer in a gravity-wave spectrum. Part II: Parameterizations of the nonlinear energy transfer for application in wave models. *J. Phys. Oceanogr.*, 15:1378–1391, 1985. URL http://journals.ametsoc.org/doi/pdf/10.1175/1520-0485%281985%29015%3C1378%3ACAPOTN%3E2.0.CO%3B2.

T. H. Il-Ju Moon, I. Ginis, S. E. Belcher, and H. L. Tolman. Effect of surface waves on air-sea momentum exchange. Part I: Effect of mature and growing seas. *J. Atmos. Sci.*, 61(19):2321–2333, 2004.

P. A. E. M. Janssen. Quasi-linear theory of wind wave generation applied to wave forecasting. *J. Phys. Oceanogr.*, 21:1631–1642, 1991. URL http://journals.ametsoc.org/doi/pdf/10.1175/1520-0485%281991%29021%3C1631%3AQLTOWW%3E2.0.CO%3B2. See comments by D. Chalikov, J. Phys. Oceanogr. 1993, vol. 23 pp. 1597–1600.

F. Leckler, F. Ardhuin, N. Reul, B. Chapron, and J.-F. Filipot. estimation of breaking crest density and whitecap coverage from a numerical wave model. In *Proceedings, 12th Int. Workshop of Wave Hindcasting and Forecasting, Hawaii*, 2011.

O. M. Phillips. On the response of short ocean wave components at a fixed wavenumber to ocean current variations. *J. Phys. Oceanogr.*, 14:1425–1433, 1984. URL http://journals.ametsoc.org/doi/pdf/10.1175/1520-0485%281984%29014%3C1425%3AOTROSO%3E2.0.CO%3B2.

P. Queffeulou and D. Croizé-Fillon. Global altimeter SWH data set, version 7, may 2010. Technical report, Ifremer, 2010. URL ftp://ftp.ifremer.fr/ifremer/cersat/products/swath/altimeters/waves/documentation/altimeter_wave_merge__7.0.pdf. URL:http://tinyurl.com/2cj5sez.

Y. Quilfen, D. Vandemark, B. Chapron, H. Feng, and J. SienkiewiCZ. Estimating gale to hurricane force winds using the satellite altimeter. *J. Atmos. Ocean Technol.*, 28:453–458, 2011.

A. Reniers, M. Groenewegen, K. Ewans, S. Masterton, G. Stelling, and J. Meek. Estimation of infragravity waves at intermediate water depth. *Coastal Eng.*, 57:52–61, 2010.

S. Saha, S. Moorthi, H.-L. Pan, X. Wu, J. Wang, S. Nadiga, P. Tripp, R. Kistler, J. Woollen, D. Behringer, H. Liu, D. Stokes, R. Grumbine, G. Gayno, J. Wang, Y.-T. Hou, H. ya Chuang, H.-M. H. a. J. S. Juang, M. Iredell, R. Treadon, D. Kleist, P. V. Delst, D. Keyser, J. Derber, M. Ek, J. Meng, H. Wei, R. Yang, S. Lord, H. van den Dool, A. Kumar, W. Wang, C. Long, M. Chelliah, Y. Xue, B. Huang, J.-K. Schemm, W. Ebisuzaki, R. Lin, P. Xie, M. Chen, S. Zhou, W. Higgins, C.-Z. Zou, Q. Liu, Y. Chen, Y. Han, L. Cucurull, R. W. Reynolds, G. Rutledge, and M. Goldberg. The NCEP Climate Forecast System Reanalysis. *Bull. Amer. Meterol. Soc.*, 91:1015–1057, 2010.

H. L. Tolman and D. Chalikov. Source terms in a third-generation wind wave model. *J. Phys. Oceanogr.*, 26: 2497–2518, 1996. URL http://journals.ametsoc.org/doi/pdf/10.1175/1520-0485%281996%29026%3C2497%3ASTIATG%3E2.0.CO%3B2.

H. L. Tolman, M. L. Banner, and J. M. Kaihatu. The NOPP operational wave improvement project. In *Proceedings, 12th Int. WOrkshop of Wave Hindcasting and Forecasting, Hawaii*, 2011.

N. Tran, D. Vandemark, S. Labroue, H. Feng, B. Chapron, H. L. Tolman, J. Lambin, and N. Picot. The sea state bias in altimeter sea level estimates determined by combining wave model and satellite data. *J. Geophys. Res.*, 115:C03020, 2010. doi: 10.1029/2009JC005534.

D. Vandemark, B. Chapron, J. Sun, G. H. Crescenti, and H. C. Graber. Ocean wave slope observations using radar backscatter and laser altimeters. *J. Phys. Oceanogr.*, 34:2825–2842, 2004.